(1998); S. Lammich *et al.*, *Proc. Natl. Acad. Sci. U.S.A.* **96**, 3922 (1999).
5. G. Evin, K. Beyreuther, C. L. Masters, *Amyloid* **1**, 263 (1994).
6. B. De Strooper *et al.*, *Nature* **391**, 387 (1998); B. De Strooper *et al.*, *ibid.* **398**, 518 (1999).
7. M. S. Wolfe *et al.*, *ibid.* **398**, 513 (1999).
8. C. Haass *et al.*, *ibid.* **359**, 322 (1992).
9. P. Seubert *et al.*, *ibid.* **361**, 260 (1993).
10. J. Zhao *et al.*, *J. Biol. Chem.* **271**, 31407 (1996).
11. E. H. Koo and S. Squazzo, *ibid.* **269**, 17386 (1994).
12. C. Haass *et al.*, *Nature Med.* **1**, 1291 (1995).
13. A. S. C. Chyung, B. D. Greenberg, D. G. Cook, R. W. Doms, V. M. Y. Lee, *J. Cell Biol.* **138**, 671 (1997).
14. C. Haass, A. Y. Hung, M. G. Schlossmacher, D. B. Teplow, D. J. Selkoe, *J. Biol. Chem.* **268**, 3021 (1993).
15. J. Knops *et al.*, *ibid.* **270**, 2419 (1995).
16. A. E. Roher *et al.*, *ibid.* **268**, 3072 (1993).
17. G. K. Gouras *et al.*, *J. Neurochem.* **71**, 1920 (1998).
18. M. Citron *et al.*, *Neuron* **17**, 171 (1996).
19. A. Capell, D. B. Teplow, M. Citron, D. J. Selkoe, C. Haass, *Amyloid* **3**, 150 (1996).
20. M. Mullan *et al.*, *Nature Genet.* **1**, 345 (1992).
21. M. Citron *et al.*, *Nature* **360**, 672 (1992); X.-D. Cai, T. E. Golde, G. S. Younkin, *Science* **259**, 514 (1993).
22. M. Citron, D. B. Teplow, D. J. Selkoe, *Neuron* **14**, 661 (1995).
23. S. L. Ross *et al.*, *J. Biol. Chem.* **273**, 15309 (1998).
24. R. Vassar *et al.*, data not shown.
25. N. D. Rawlings and A. J. Barrett, *Methods Enzymol.* **248**, 105 (1995).
26. In situ hybridizations were performed using 10-μm sections through fresh frozen brain tissue obtained from adult Sprague-Dawley rats. Antisense riboprobes labeled with ^{35}S-UTP and ^{35}S-CTP were generated from rat BACE cDNA Bgl II–Kpn I fragment (nucleotides +815 to +1593). Hybridization and wash conditions were as described (*36*).
27. A synthetic peptide corresponding to the COOH-terminal 17 amino acids of BACE was synthesized, conjugated to keyhole limpet hemocyanin (KLH), and used to raise a polyclonal antibody. The antibody and preimmune serum (negative control) were coupled to Protein A Sepharose for use in immunoprecipitation assays. Pieces of parietal cortex of human Alzheimer's disease and control brains obtained from Sun Health Research Institute (Arizona) were homogenized in lysis buffer (*22*), and the homogenate was spun at 20,000*g* for 10 min at 4°C. For each immunoprecipitation about 25 mg wet weight equivalent were used. BACE immunoprecipitation from extracts of 293 cells transiently transfected with BACE were carried out as in (*8*), and the precipitates were subjected to SDS-PAGE followed by immunoblotting with the BACE antiserum as primary antibody.
28. For the generation of the BACE-HA cell line, a BACE-HA fusion construct was made containing the nine–amino acid hemagglutinin epitope (*37*) fused in frame at the BACE COOH-terminus.
29. Immunocytochemistry of paraformaldehyde-fixed Triton X-100 permeabilized cells followed standard protocols (*12*). Primary antibodies and dilutions were the following: anti-HA monoclonal or polyclonal antibodies (Covance) 1:100; anti-58K (Sigma) 1:20; and anti-transferrin receptor (Dako) 1:20; anti-APPsβsw 1:500. Alexa 488 (green) and Alexa 594 (red) secondary antibodies (Molecular Probes) were used at 1:200 dilution.
30. Transfection, metabolic labeling, preparation of total cell lysates, immunoprecipitation, and protein radiosequencing were carried out as in (*8*). For immunoprecipitation of APP and its COOH-terminal fragments, we used a polyclonal antibody that we raised to the last 20 amino acids of the cytoplasmic tail of APP. For immunoprecipitation of Aβ we used the monoclonal antibody 4G8 raised to Aβ17-24 (Senetek). Quantitation of APP metabolites was done using time-resolved fluorescence sandwich ELISA assays with unmodified capture antibody and a biotinylated reporter antibody. Europium-labeled streptavidin was then reacted with the biotinylated antibody and the europium was quantitated by Delfia time-resolved fluorescence. For quantitation of total Aβ ($Aβ_{1-x}$), we established an ELISA using monoclonal antibody 4G8 as capture and biotinylated monoclonal antibody 6E10 raised to Aβ1-17 (Senetek) as reporter. This assay detects all forms of Aβ with an intact NH_2-terminus. For quantitation of all Aβ derivatives ending at amino acid 42 ($Aβ_{x-42}$), we established an ELISA using anti-Aβ 42, a purified rabbit polyclonal antibody that specifically recognizes the 42 form of Aβ (Biosource International) as capture and biotinylated 4G8 as reporter. This assay detects all forms of Aβ and p3 that end at amino acid 42. A similar ELISA for detection of $Aβ_{x-40}$ was established using anti-Aβ 40, a purified rabbit polyclonal antibody which specifically recognizes the 40 form of Aβ (Biosource International). For quantitation of APPsα we used a polyclonal antibody raised to the APP midregion (total APP) as capture and biotinylated 6E10 as reporter. For quantitation of APPsβsw, we raised a polyclonal antibody specific for the β-secretase generated neoepitope of APPsw and used this antibody as capture, followed by biotinylated monoclonal antibody 5A3 (total APP) (*11*) as reporter.
31. Z. Zhong *et al.*, *J. Biol. Chem.* **269**, 627 (1994).
32. Antisense oligonucleotides complementary to BACE mRNA were generated (Sequitur): AS#2 (5′-GUCCUGAACUCAUCGUGCACAUGGC-3′); AS#3 (5′-CAUCUGUGUCUCCUACUUGUGACCA-3′); and AS#4 (5′-CCAAGAGUAUUCCCGCCAGCAGAGU-3′). A reverse sequence control oligonucleotide for each antisense oligonucleotide was also synthesized. The following AS#2 mismatch control oligonucleotides were made: 2MIS (5′-GUCCUGAAGUCAUCGUCCACAUGGC-3′); 4MIS (5′-GUCCAGAAGUCAUCGUCCACUUGGC-3′); and 6MIS (5′-GGCCAGAAGUCAUCGUCCACUUGUC-3′). The APPsw cells were plated in 6-well dishes at 396,000 cells/well. After reaching ~70 to 80% confluency, cells were treated in triplicate with antisense or control oligonucleotide continuously for 48 hours in the presence of serum using a lipid delivery system (Sequitur). Cells were then washed and fresh medium was added for 6 to 8 hours of conditioning. Conditioned media were collected and assayed by APPsβsw, APPsα, Aβx-40, and Aβx-42 ELISAs. In addition, cells from triplicate wells were harvested and pooled for isolation of polyadenylated [poly(A)$^+$] RNA (Micro-FastTrack; Invitrogen). Northern analysis was performed as described above. For normalization, blots were stripped and reprobed with phospholipase A2 and glyceraldehyde-3 phosphate dehydrogenase cDNA probes (Clonetech; Palo Alto, CA). Blots were visualized and quantitated using a Storm 860 phosphoImager (Molecular Dynamics).
33. For the soluble BACE-IgG cell line, we generated a fusion construct encoding BACE amino acids 1–460 (ending at the start of the predicted transmembrane sequence) fused in frame with a three–amino acid linker (alanine-valine-threonine) and the Fc portion of human IgG1 (starting at amino acid 29; GenBank accession number X70421). BACE-IgG was purified from conditioned media of stably transfected 293T cells with Protein A columns. Substrate peptides were synthesized and labeled with dinitrophenol at P8′ to allow easy ultraviolet detection of cleavage products after reversed phase high performance liquid chromatography. The APPwt substrate sequence was TTRPGSGLTNIKTEEISEVKMDAEFRHDK(dnp)G; in the Swedish mutant variant, KM is substituted by NL, and in the MV mutant, M is substituted by V. All assays were performed with the same batch of BACE-IgG. Substrates were used at 30 μM in a 50-μl assay. All assays were buffered with 50 mM acetic acid (pH 4.5) unless otherwise indicated. Enzyme and substrate were incubated between 30 min and 18 hours at room temperature, then the reaction mixtures were quenched and analyzed by reversed-phase HPLC. Both product and substrate were monitored by absorbance at 360 nm. Products were identified by retention time comparison with a reference peptide run under identical conditions.
34. M. P. Murphy *et al.*, *J. Biol. Chem.* **274**, 11914 (1999).
35. D. Games *et al.*, *Nature* **373**, 523 (1995).
36. E. J. Curran and S. J. Watson, *J. Comp. Neurol.* **361**, 57 (1995).
37. J. Field *et al.*, *Mol. Cell Biol.* **8**, 2159 (1988).
38. Single-letter abbreviations for the amino acid residues are as follows: A, Ala; C, Cys; D, Asp; E, Glu; F, Phe; G, Gly; H, His; I, Ile; K, Lys; L, Leu; M, Met; N, Asn; P, Pro; Q, Gln; R, Arg; S, Ser; T, Thr; V, Val; W, Trp; and Y, Tyr. X indicates any residue.
39. We thank E. H. Koo for monoclonal antibody 5A3, T. Woolf for technical advice on antisense experiments, G. Zajic for help with microscopy, and N. Davidson, T. Livelli, and J. Ngai for helpful discussions. We also thank D. Paulin, D. Olivares, and G. Zajic for preparation of figures.

10 September 1999; accepted 27 September 1999

Contact-Dependent Inhibition of Cortical Neurite Growth Mediated by Notch Signaling

Nenad Šestan,[1] Spyros Artavanis-Tsakonas,[2] Pasko Rakic[1]*

The exuberant growth of neurites during development becomes markedly reduced as cortical neurons mature. In vitro studies of neurons from mouse cerebral cortex revealed that contact-mediated Notch signaling regulates the capacity of neurons to extend and elaborate neurites. Up-regulation of Notch activity was concomitant with an increase in the number of interneuronal contacts and cessation of neurite growth. In neurons with low Notch activity, which readily extend neurites, up-regulation of Notch activity either inhibited extension or caused retraction of neurites. Conversely, in more mature neurons that had ceased their growth after establishing numerous connections and displayed high Notch activity, inhibition of Notch signaling promoted neurite extension. Thus, the formation of neuronal contacts results in activation of Notch receptors, leading to restriction of neuronal growth and a subsequent arrest in maturity.

Cerebral cortical neurons grow by extending neurites (that is, axons and dendrites) and forming connections until they reach a mature size, at which their capacity to grow and remodel their connections becomes markedly reduced (*1*). The molecular mechanisms that regulate

the transition from growth to stability remain obscure. Here, we provide evidence in vitro that Notch signaling is involved in this transition by regulating the capacity of cortical neurons to extend and elaborate neurites.

Notch receptors and ligands are localized to cortical neurites. The Notch pathway is an evolutionarily conserved cell-cell signaling mechanism involved in cell fate decisions during different cellular and developmental processes (*2*–*4*), including neural development (*5*). The first indication that Notch signaling plays a role in postmitotic differentiation of cortical neurons was that Notch1 and Notch2 receptors, and their ligands Delta1 and Jagged2 (*4*), were expressed throughout the cerebral cortex and localized to neuronal bodies, neurites, and synapses (*6, 7*).

Nuclear localization of the intracellular domain of Notch in neurons. Because the proteolytic cleavage and nuclear translocation of the intracellular portion of Notch are thought to be important for receptor signaling (*8, 9*), we examined the subcellular distribution of Notch intracellular domain (ICD) epitopes in the developing and adult mouse cerebral cortex (*6*). At embryonic day 16 (E16), Notch1 ICD, and to a lesser extent Notch2 ICD, epitopes were distributed throughout the entire cytoplasm (excluding the nuclei) of proliferating cells in the ventricular and subventricular zones, as well as in migrating neurons in the intermediate zone (Fig. 1, A to B′ and F to G′). In contrast, the nuclei of early-generated neurons situated in the middle and lower thirds of the cortical plate showed staining for Notch1 and Notch2 ICD (Fig. 1, C and H). Newly arrived and less mature neurons in the upper third of the cortical plate, as well as neurons migrating between the earlier generated and already settled neurons, lacked appreciable amounts of nuclear Notch (Fig. 1, C, C′, H, and H′). However, because almost all cortical neurons of the postnatal day 7 (P7) and adult mouse exhibited nuclear staining for Notch1 and Notch2 ICD (Fig. 1, D, E, I, and J), we assumed that all cortical neurons eventually acquired nuclear Notch. The lack of nuclear staining with antibodies to extracellular epitopes of Notch (*10*) is consistent with the notion that the ICD is cleaved and translocated to the nuclei of postmigratory neurons during the period of dendritic growth and increase in cell-cell contacts. In neuronal cells lacking detectable nuclear Notch, nuclear ICD-dependent signaling could still occur, requiring very small amounts of ICD that are undetectable by conventional immunohistochemistry (*9*). Alternatively, nuclear translocation of the ICD may not be necessary and thus not strictly correlated with Notch signaling (*3, 11*).

Notch activation and nuclear localization depend on cell-cell contacts. To test whether Notch is activated and translocated to the nucleus as a result of receptor-ligand interactions among neurons contacting each other, we cultured dissociated cortical neurons from E15–16 mouse embryos and then performed assays for the localization of Notch ICD epitopes and the degree of endogenous Notch activity over time. Two different plating densities were used—low density (LD; 15×10^3 cells/cm^2) and high density (HD; 150×10^3 cells/cm^2)—so as to vary the number of cell-cell contacts (*12*). In both LD and HD cultures, neurons expressing Notch, Delta, and Jagged began to extend their processes within a few hours of plating (*10*). Endogenous Notch ICD immunoreactivity was observed in cell bodies and along the entire length of extending neurites, including growth cones (*6*) (Fig. 2, A and B). By the second day in vitro (2 DIV), neurons in HD cultures exhibited moderate amounts of nuclear Notch, which increased until 7 DIV, when strong immunoreactivity was detected in all neurons (Fig. 2, E and F). In contrast, most neurons in LD cultures did not have appreciable amounts of nuclear Notch during the first week in vitro (Fig. 2, C and D). Most neurons in the densely packed E15–16 cortical plate exhibited nuclear staining (Fig. 1, C and H), which suggests that culturing at LD—where neurons generally do not contact each other during the first few days—resulted in a loss of the nuclear Notch. Only by 9 DIV (Fig. 2, G and H) did neurons in LD cultures exhibit moderate amounts of nuclear Notch, when presynaptic boutons were also apparent on neurons that stained for Notch (Fig. 1, G′ and H′). In contrast, in HD cultures, synapses were present much earlier (*10*), indicating that more contacts developed among neurons in HD than in LD cultures during the first week in vitro.

[1]Section of Neurobiology, Yale University School of Medicine, New Haven, CT 06510, USA. [2]Massachusetts General Hospital Cancer Center, Department of Cell Biology, Harvard Medical School, Charlestown, MA 02129, USA.

*To whom correspondence should be addressed. E-mail: pasko.rakic@yale.edu

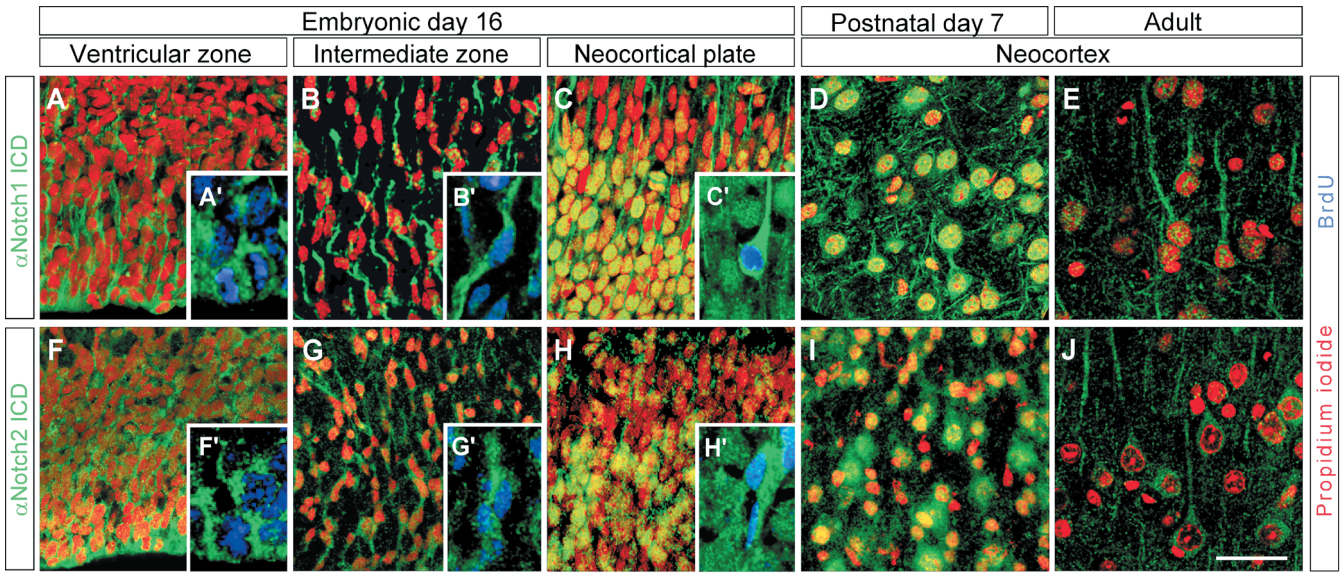

Fig. 1. Subcellular distribution of Notch ICD epitopes imaged by confocal microscopy. (**A** to **C**, **F** to **H**) Notch ICD immunostaining (green) of neuronal progenitors shows a honeycomb-like pattern, whereas in the neocortical plate it exhibits a mosaic-like pattern. (**A′** to **C′**, **F′** to **H′**) Timed-pregnant mice ($n = 2$) received three BrdU (blue) injections at 0, 10, and 16 hours (*36*) to identify proliferative cells and selectively label newly generated neurons. Twenty-four hours later, embryos ($n = 4$) were fixed and immunostained. (**D**, **E**, **I**, and **J**) Notch ICD immunostaining in layer 5 neurons of the P7 and adult somatosensory neocortex. Cell nuclei were stained with propidium iodide (red). Scale bar, 50 μm.

The activation of Notch receptors in neuronal progenitors induces the C-promoter binding factor 1 (CBF1)–dependent transactivation of *HES1* and *HES5* genes (*5*). Because *HES* genes are also expressed in cortical neurons (*13*), we examined whether the formation of contacts and the presence of nuclear Notch correlate with the CBF1-dependent transactivation of *HES* genes in neurons. First, we measured the transactivation of a 4xwtCBF1-luciferase reporter construct (CBF1-luc) in the transiently transfected neurons (*14, 15*) as an indicator of endogenous Notch activity (*16, 17*). Relative to the baseline we selected (the CBF1-luc activity from LD cultures at 2 DIV), we found that neurons from HD culture at 2 DIV had 25.5 ± 0.7 times as much Notch activity ($P = 0.0008$). Furthermore, Notch activity in both LD and HD cultures increased with time (Fig. 2I). For example, relative to the baseline, at 9 DIV there was 24.72 ± 0.29 times as much Notch activity in neurons from LD cultures ($P = 0.0001$) and 183.27 ± 20.69 times as much Notch activity in neurons from HD cultures ($P = 0.003$). Notably, the degree of Notch activity in neurons from the 9 DIV LD cultures equaled that in neurons from the 2 DIV HD cultures ($P = 0.41$); this suggests that Notch activity did not depend on time in vitro, but rather on the number of interneuronal contacts. Similarly, *HES1* and *HES5* transcripts were detected in HD cultures by the reverse transcription polymerase chain reaction (RT-PCR) (*18*) at 2 DIV, where-

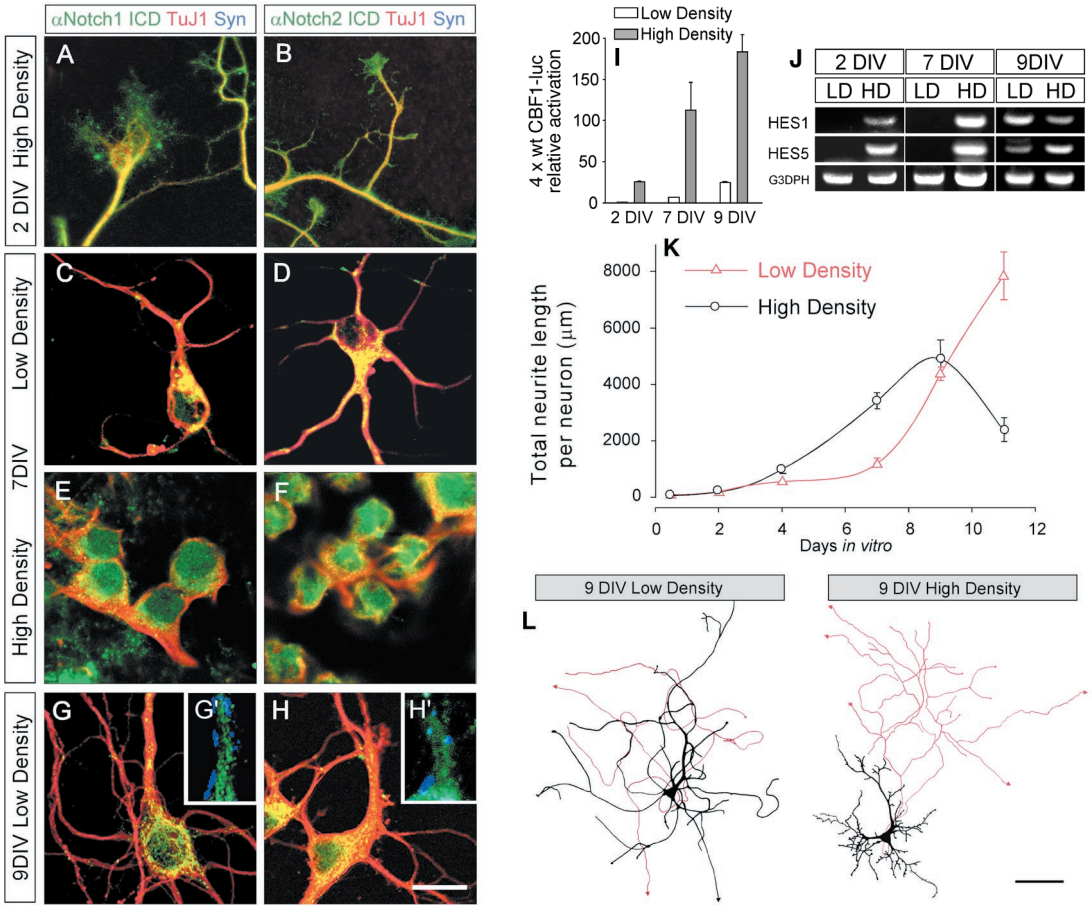

Fig. 2. Effect of neuronal density on Notch activity and neurite growth. (**A** to **H**) Confocal images of Notch1 and Notch2 ICD immunostaining (green) of TuJ1$^+$ neurons (red). (**G′** and **H′**) Notch ICD$^+$ dendrites are dotted with synaptophysin-labeled (blue) presynaptic boutons, which generally lack appreciable Notch staining. (**I**) Time course of normalized CBF1-luc transactivation in LD and HD cultures. (**J**) RT-PCR analysis of *HES* expression ($n = 3$ trials). (**K**) Changes in total neurite length per neuron over time. For LD cultures, EGFP-transfected and TuJ1$^+$ neurons were not significantly different ($P > 0.08$) and were thus pooled together. Neurons in HD cultures at 7 and 9 DIV were not significantly different ($P = 0.09$); neurons at 11 DIV were smaller than neurons at 9 DIV ($P = 0.03$). At 9 DIV, neurons from LD and HD cultures were not significantly different ($P = 0.35$). (**L**) Reconstruction of two representative pyramidal neurons. Black, dendrites; red, axons. Data in (I) and (K) are means ± SEM ($n \geq 3$ trials). Scale bars, 5 μm (A and B), 20 μm (C to H), 100 μm (L).

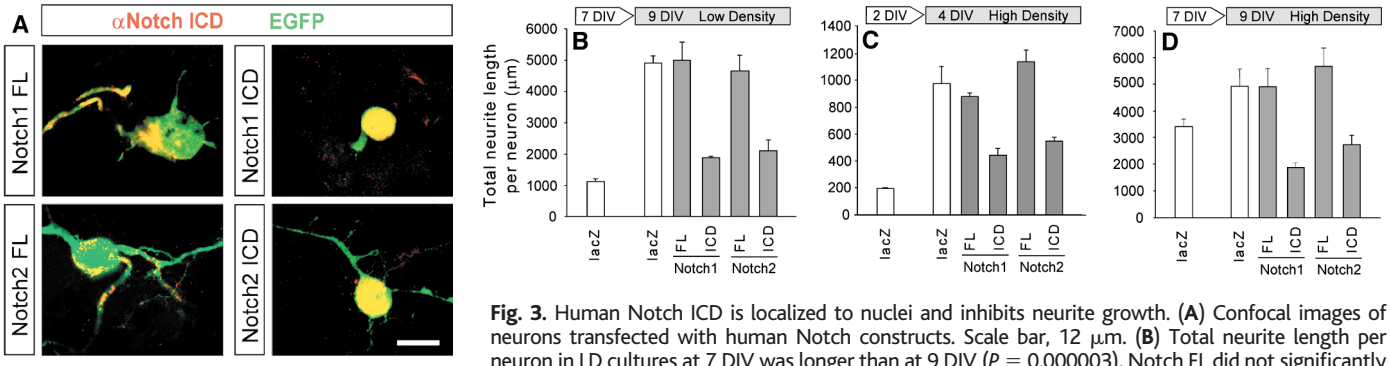

Fig. 3. Human Notch ICD is localized to nuclei and inhibits neurite growth. (**A**) Confocal images of neurons transfected with human Notch constructs. Scale bar, 12 μm. (**B**) Total neurite length per neuron in LD cultures at 7 DIV was longer than at 9 DIV ($P = 0.000003$). Notch FL did not significantly affect neurite growth ($P > 0.61$). Notch ICD inhibited neurite growth ($P \leq 0.0001$). (**C**) In HD cultures, 4 DIV neurons had greater total neurite length than 2 DIV neurons ($P = 0.003$). Notch FL did not significantly affect neurite growth ($P > 0.35$). Notch ICD inhibited neurite growth ($P \leq 0.01$). (**D**) Total neurite lengths per neuron in HD cultures at 7 and 9 DIV were not significantly different ($P = 0.09$). Notch FL did not significantly affect the total neurite length ($P > 0.47$). Notch1 ICD caused neurite retraction in 7 DIV neurons ($P = 0.0037$). Notch2 ICD inhibited the neurite growth ($P = 0.017$) but did not cause significant retraction of neurites ($P = 0.19$) in 7 DIV cultures. Data in (B) to (D) are shown as means ± SEM ($n \geq 5$ trials).

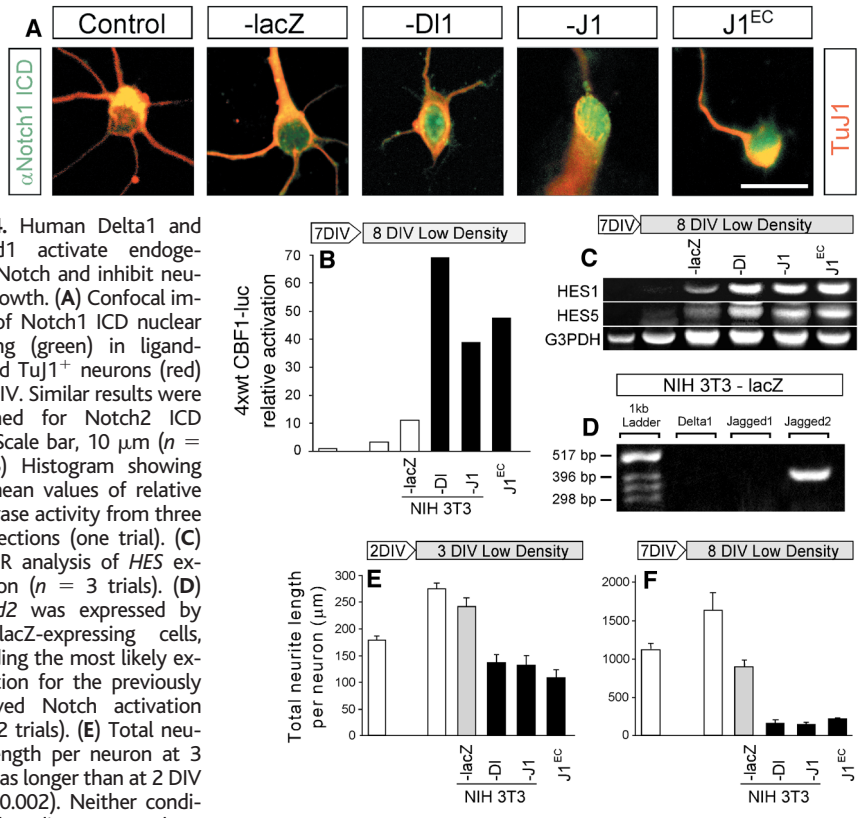

Fig. 4. Human Delta1 and Jagged1 activate endogenous Notch and inhibit neurite growth. (**A**) Confocal images of Notch1 ICD nuclear staining (green) in ligand-treated TuJ1^{+} neurons (red) at 8 DIV. Similar results were obtained for Notch2 ICD (*10*). Scale bar, 10 μm (n = 3). (**B**) Histogram showing the mean values of relative luciferase activity from three transfections (one trial). (**C**) RT-PCR analysis of *HES* expression (n = 3 trials). (**D**) *Jagged2* was expressed by the lacZ-expressing cells, providing the most likely explanation for the previously observed Notch activation (n = 2 trials). (**E**) Total neurite length per neuron at 3 DIV was longer than at 2 DIV ($P < 0.002$). Neither conditioned medium nor coculturing with lacZ-expressing cells significantly affected neurite growth ($P > 0.14$). Dl1 and J1 ($P \leq 0.003$) cells inhibited the neurite growth but did not cause significant retraction ($P > 0.055$). J1^{EC}-enriched medium caused neurite retraction ($P = 0.011$). (**F**) Total neurite length per neuron at 8 DIV was not significantly longer than at 7 DIV ($P = 0.08$). lacZ-expressing cells inhibited neurite growth ($P = 0.01$), probably because of endogenous ligand expression (D). Dl1 and J1 cells ($P \leq 0.00003$) and J1^{EC}-enriched medium ($P = 0.00003$) caused retraction of neurites. Data in (E) and (F) are means ± SEM (n = 3 trials).

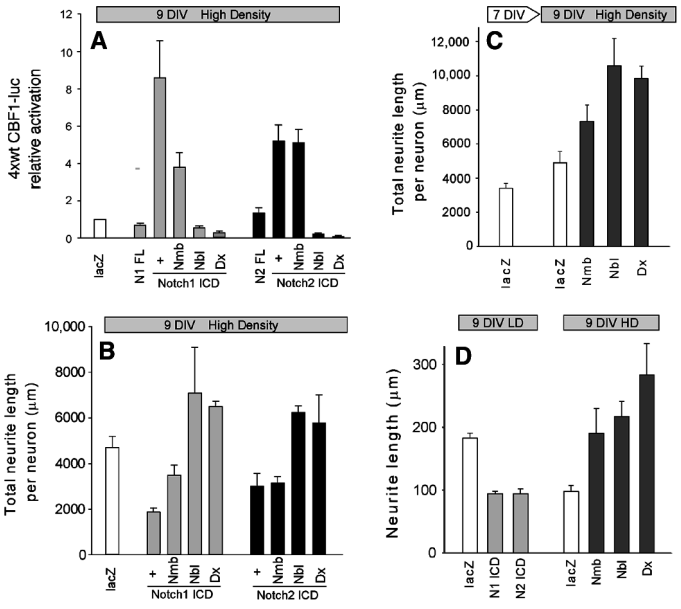

Fig. 5. Nmb, Nbl, and Dx inhibit Notch activity and promote neurite extension. (**A**) Notch ICD transactivated CBF1-luc ($P < 0.004$). Nmb partially inhibited Notch1 ICD activity ($P = 0.01$) but did not significantly inhibit Notch2 ICD activity ($P = 0.93$). Notch ICD transactivation of CBF1-luc was inhibited by Nbl and Dx ($P \leq 0.002$). Nbl and Dx also inhibited endogenous Notch activity ($P \leq 0.007$). (**B**) Nmb partially rescued the effect of Notch1 ICD ($P = 0.01$) but did not significantly change the effect of Notch2 ICD ($P = 0.52$) on neurites. Notch1 and Notch2 ICD effects were rescued by Nbl ($P = 0.027$ and $P = 0.002$) and Dx ($P < 0.00005$ and $P = 0.02$). (**C**) Total neurite length per neuron in HD cultures did not significantly increase between 7 and 9 DIV ($P = 0.09$). Nbl and Dx ($P \leq 0.007$), but not Nmb ($P = 0.06$), induced an increase in total neurite length per neuron. (**D**) Notch ICD decreased the mean neurite length in LD cultures ($P = 0.0001$), whereas Nmb ($P = 0.03$), Nbl ($P = 0.001$), and Dx ($P < 0.005$) increased the mean neurite length in HD cultures. All data are means ± SEM ($n \geq 3$ trials).

as in LD cultures they were not detected until 9 DIV (Fig. 2J).

Contact-dependent inhibition of neurite growth. Consistent with previous reports that the rates of neurite extension and synaptogenesis depend on interneuronal contacts (*19*), neurons in HD cultures extended their processes more rapidly than in LD cultures (Fig. 2K) (*14, 20*). However, neurons in HD cultures also stopped growing earlier and even partially retracted their neurites after 9 DIV. Conversely, neurons in LD cultures initially grew more slowly, but still achieved the same total neurite length as those in HD cultures by 9 DIV. Moreover, in contrast to HD cultures, neurons in LD cultures continued to grow after 9 DIV. Neurons in the LD cultures also had longer and "smoother" neurites with few branches at 9 DIV, whereas neurons in HD cultures had much shorter neurites and a "bushier" morphology (Fig. 2L). Finally, Notch activity in neurons from HD cultures was 7.42 ± 0.83 times that in neurons from LD cultures at 9 DIV ($P = 0.005$) (Fig. 2I), indicating that the increase in Notch activity was concomitant with the restriction in the growth capacity of neurons in the HD cultures.

Constitutively active Notch ICD inhibits neurite growth. To test whether Notch signaling plays a role in restricting neurite growth, we induced Notch activity by transfecting neurons (*14*) with plasmids encoding truncated forms of human Notch1 and Notch2 containing the entire ICD. After transfection, the Notch ICD products were predominantly localized to the nuclei, whereas products of the control construct encoding the full-length (FL) Notch were localized to the cytoplasm and neurites (Fig. 3A). Cotransfection with *CBF1-luc* revealed strong transactivation with the ICD but not the FL form of *Notch* (Fig. 5A), consistent with the notion that the ICD acts as a constitutively active receptor capable of interacting with endogenous CBF1 and stimulating transcription (*16, 17*).

The effect of Notch1 and Notch2 ICD on neurite growth was first examined in LD cultures at 7 DIV, when they exhibit maximum growth and display little endogenous Notch activity (Fig. 2, I and K). When total neurite length per neuron was measured 48 hours after transfection (*20*), Notch FL had not significantly affected the neurite growth (Fig. 3B), whereas Notch ICD had stopped it. To examine whether the effect of Notch ICD correlated with the degree of Notch activity or the age of the neurons, we transfected neurons in the HD cultures at 2 DIV. These neurons were 5 days younger, in the phase of extensive neurite growth, and displayed little Notch activity (Fig. 2, I and K). Similar to the growth arrest observed in the LD culture neurons at 7 DIV (Fig. 3B), expression of Notch ICD in the HD culture neurons at 2 DIV arrested the growth of neurites (Fig. 3C). Finally, we increased the already

high Notch activity in the HD culture neurons at 7 DIV, which had established neurites and ceased growing (Fig. 2, I and K), and found that expression of Notch1 ICD, and to a lesser extent Notch2 ICD, caused a premature retraction of neurites, normally observed only after 9 DIV (Fig. 3D). Thus, low Notch activity did not arrest the growth of neurites, whereas higher amounts either prematurely inhibited neurite growth or caused their retraction in a dose-dependent manner, independent of the age of neurons.

Notch ligand-dependent inhibition of neurite growth. Next, we examined whether the Notch receptors could be activated in a ligand-dependent fashion and whether large amounts of ligands in the LD cultures could mimic the growth inhibition evident in the HD cultures (Fig. 2K) or induced by Notch ICD (Fig. 3B). Recent in vitro studies have shown that exogenously applied ligands can activate endogenous Notch receptors and mimic the effects of Notch ICD (*21–24*). Thus, neurons in a LD culture were either cocultured with stably transfected *Delta1* (Dl1) and *Jagged1* (J1)–expressing cells or cultured in the presence of conditioned medium enriched with a soluble form of human Jagged1 ($J1^{EC}$) (*25*). In control neurons, Notch ICD immunofluorescent signals were predominantly localized perinuclearly. In contrast, nuclear staining was observed in neurons receiving ligand treatment (Fig. 4A). Consistently, strong transactivation of CBF1-luc (*15*) and the induction of *HES* expression (*18*) were detected in these neurons (Fig. 4, B and C).

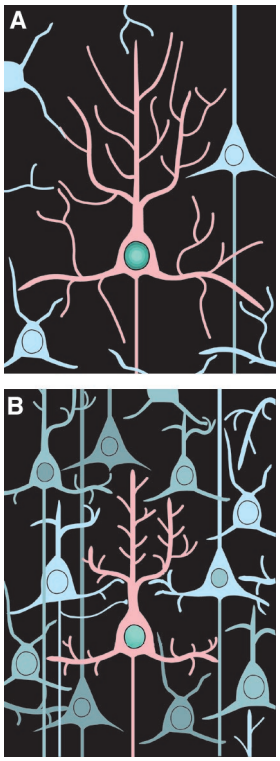

Fig. 6. Model of contact-dependent regulation of neurite growth by Notch. (**A**) In LD cultures, where the Notch present on neurites does not have access to ligands on distant neurons (blue), the neuron (pink) is able to extend its neurites farther. (**B**) In HD cultures, where Notch gains access to ligands by contacting numerous neighboring neurons (blue), neurite extension (pink) is more inhibited than in LD cultures.

Neurite growth was inhibited in LD cultures at 2 DIV when cocultured with Dl1 and J1 cells as well as when cultured in $J1^{EC}$-enriched medium (Fig. 4E) (*20*). However, at 7 DIV, the same ligand treatment caused the retraction of neurites (Fig. 4F) in a manner reminiscent of the neurite retraction in the HD cultures. Thus, exposure to large amounts of ligands mimics the effects of HD cultures and Notch ICD expression on neurite growth, indicating that the contact-dependent inhibition of neurite growth can be mediated by Notch-ligand interactions among neighboring cells.

Antagonizing Notch activity promotes neurite extension. To corroborate the notion that the growth-inhibiting effect on neurons in HD culture at 9 DIV is due to activation of endogenous Notch, we examined the effect of antagonizing the Notch activity on neurite growth. Intracellular modulators of Notch signaling, Numb (Nmb), Numb-like (Nbl), and Deltex (Dx) affect Notch signaling presumably by binding the ICD and are expressed in the developing brain (*26–28*). When cotransfected with *Notch ICD* into neurons, *nmb, nbl*, and *dx* inhibited Notch activity (Fig. 5A). Interestingly, Nmb inhibited the Notch1 ICD but not the Notch2 ICD transactivation of CBF1-luc. Conversely, Nbl and Dx abolished CBF1-luc transactivation by Notch1 and Notch2 ICD, reducing it to ~10% of the endogenous baseline Notch activity. Similarly, Nmb partially rescued the retraction of neurites caused by Notch1 ICD but did not significantly alter the effect of Notch2 ICD. On the other hand, Nbl and Dx completely rescued the retraction of neurites caused by the transfection of either Notch1 or Notch2 ICD (Fig. 5B). Next, to determine whether expression of *nmb, nbl,* or *dx* would reverse endogenous Notch-induced inhibition of growth and thus reinitiate neurite extension in neurons that had ceased growth, we transfected the HD culture neurons at 7 DIV with corresponding expression constructs (*14*). We found that Nbl and Dx promoted neurite growth, whereas Nmb did not significantly increase the total neurite length (Fig. 5C). Notably, neither of the modulators prevented the nuclear translocation of Notch ICD (*7*), suggesting that the ICD is modified, directly or indirectly, so that its signal is blocked in the nucleus or locally within neurites, or both. These results also indicate that Nmb may act as a differential modulator of Notch receptors and that the function of Dx, which can facilitate Notch signaling (*28*), may depend on the cellular and developmental context (*3, 29*).

Finally, we determined whether the expression of Notch and its signaling modulators affects the extension of existing neurites or the outgrowth of new ones (*20*). In LD cultures analyzed at 9 DIV, Notch ICD decreased the mean neurite length (Fig. 5D), causing the neurons to grow shorter and more branched neurites, and making them appear more like neurons in HD culture. Conversely, Nmb, Nbl, and Dx increased the mean neurite length in the HD culture neurons analyzed at 9 DIV (Fig. 5D), which indicates that they promoted the extension of existing neurites, causing neurons to grow longer and less branched neurites, and making them appear more like neurons in LD cultures (see Fig. 2L). These results are consistent with the notion that contact-dependent Notch activation by neighboring neurons mediates the growth arrest of neurons in HD cultures and that Notch regulates the morphological development of neurons by affecting the extension of existing neurites.

Notch regulates postmitotic differentiation and neuronal size. Our results show that contact-dependent Notch-ligand interactions among neighboring neurons mutually restrict their neurite growth and affect their final size (Fig. 6). Notably, neurite growth and the final size of a dendritic field depend on local cell-cell interactions and neuronal density (*30*). The effect of Notch on neurite growth depends critically on the degree of Notch activity. Low Notch activity may even be permissive for growth by directly or indirectly stabilizing the structure of existing neurites, whereas high Notch activity would be expected to inhibit neurite growth. Furthermore, recent studies have shown that the members of the Notch signaling pathway affect neuronal differentiation and neurite outgrowth (*31*).

Given that members of the Notch signaling pathway are expressed in neurons of the adult cerebral cortex, it is plausible that Notch plays a role in maintaining the stability of neurites and connections. It is also likely that an alteration in Notch activity would contribute to the distortion of neurites in neurological diseases. For example, Alzheimer's disease is caused by mutations in presenilins (*32*), which are required for Notch cleavage and activity (*33*). Taken together, these results suggest that changes in Notch activity contribute to differences in neuronal capacity to grow and differentiate.

References and Notes

1. P. Rakic and P. S. Goldman-Rakic, Eds., *Development and Modifiability of the Cerebral Cortex* (MIT Press, Cambridge, MA, 1982); T. N. Wiesel, *Nature* **299**, 583 (1982); A. M. Craig and G. Banker, *Annu. Rev. Neurosci.* **17**, 267 (1994); H. W. Horch, A. Kruttgen, S. D. Portbury, L. C. Katz, *Neuron* **23**, 353 (1999).
2. J. Kimble and P. Simpson, *Annu. Rev. Cell. Dev. Biol.* **13**, 333 (1997); I. Greenwald, *Genes Dev.* **12**, 1751 (1998).
3. S. Artavanis-Tsakonas, M. D. Rand, R. J. Lake, *Science* **284**, 770 (1999).
4. T. Gridley, *Mol. Cell. Neurosci.* **9**, 103 (1997); G. Weinmaster, *ibid.*, p. 91.

5. P. Beatus and U. Lendahl, *J. Neurosci. Res.* **54**, 125 (1998); I. Ahmad, P. Zagouras, S. Artavanis-Tsakonas, *Mech. Dev.* **53**, 73 (1995).
6. Fixed frozen sections and cells were preincubated in blocking solution [BS; 5% donkey serum, 1% bovine serum albumin, 0.1% glycine, 0.1% L-lysine, 0.4% Triton X-100 in phosphate-buffered saline (PBS)] for 1 hour at room temperature, and left overnight at 4°C in primary antibodies/BS: bTAN20, bhN6D [1:5 (*29, 34*)]; PGHN [1:1200 (*34*)]; IC [1:800; F. Logeat *et al*., *Proc. Natl. Acad. Sci. U.S.A.* **95**, 8108 (1998)]; 88-C (1:2000), J59 [1:1000 (*23*)]; TS1 [1:5 (*35*)]; NotchC-20, JaggedC-20 (1:250, Santa Cruz); TuJ1 (1:500, BAbCO); anti-synaptophysin (1:200, Sigma); and anti-BrdU (1:75, Becton-Dickinson)]. After washing in PBS, samples were incubated with Cy2, Cy3, and Cy5 conjugated secondary antibodies (1:300, Jackson Immunoresearch) for 45 min. Single optical images were collected on a MRC 1024 confocal microscope (Bio-Rad).
7. Supplement Web material is available at www.sciencemag.org/feature/data/1042942.shl.
8. M. Lecourtois and F. Schweisguth, *Curr. Biol.* **8**, 771 (1998); G. Struhl and A. Adachi, *Cell* **93**, 649 (1998).
9. E. H. Schroeter, J. A. Kisslinger, R. Kopan, *Nature* **393**, 382 (1998).
10. N. Šestan, thesis, Yale University (1999).
11. J. C. Aster *et al*., *J. Biol. Chem.* **272**, 11336 (1997).
12. Dorsal telencephalon was dissociated with 0.01% papain (Worthington), 0.1% neutral protease (Roche), and 0.01% DNase I (Sigma) in Hanks' balanced salt solution twice for 15 min at 37°C, and gently triturated. Single cells were resuspended in Neurobasal medium containing 2% B27, 5% fetal bovine serum (FBS), 2 mM L-glutamine, 1 mM sodium pyruvate, penicillin (100 U/ml), and streptomycin (100 μg/ml) (all from Gibco), plated on precoated glass cover slips (*24*) at LD and HD, and incubated at 37°C in 5% CO_2.
13. C. Akazawa, Y. Sasai, S. Nakanishi, R. Kageyama, *J. Biol. Chem.* **267**, 2187 (1992); Y. Sasai, R. Kageyama, Y. Tagawa, R. Shigemoto, S. Nakanishi, *Genes Dev.* **6**, 2620 (1992).
14. The Helios Gene Gun (Bio-Rad) was used to transfect neurons with CMV-based plasmids [phN1 FL, pNotch1 FL, pNotch1 ICD (amino acids 1758 to 2556), pNotch2 FL, pNotch2 ICD (amino acids 1701 to 2471) (*24, 34*); pnumb, pnumb-like (*26*); pdeltex, p4xwtCBF1-luc (*29*); pEGFP-N2 (Clontech); placZ]. DNA was precipitated onto ~35 mg of 1-μm gold microcarrier. Coprecipitation ratios: 25 μg of pEGFP-N2 1:3 with placZ or 1:1.5:1.5 with other plasmids; and 33 μg of p4xwtCBF1-luc 1:3 with placZ or 1:1:1 with other plasmids, to a total of 100 μg. The DNA was delivered into neurons at ~100 psi. Neurons were analyzed 48 hours after transfection. Enhanced green fluorescent protein (EGFP) autofluorescence was evenly distributed along the entire neurite. EGFP/lacZ coprecipitation resulted in ~95% efficiency of coexpression as early as 12 to 15 hours after transfection.
15. The cells were washed with PBS and lysed in 50 μl of lysis buffer. Cell extract (10 μl) was used to measure either luciferase activity or β-galactosidase activity.
16. J. J.-D. Hsieh *et al*., *Mol. Cell. Biol.* **16**, 952 (1996); F. M. Lu and S. E. Lux, *Proc. Natl. Acad. Sci. U.S.A.* **93**, 5663 (1996); J. J.-D. Hsieh, D. E. Nofziger, G. Weinmaster, S. D. Hayward, *J. Virol.* **71**, 1938 (1997).
17. D. Nofziger, A. Miyamoto, K. M. Lyons, G. Weinmaster, *Development* **126**, 1689 (1999).
18. For RT-PCR (Titan System, Roche), 100 ng of total RNA were isolated using TRIZOL (Gibco). Typical PCR cycle parameters were as follows: *HES* analysis, 5 min at 95°C, 45 s at 58°C, and 1.5 min at 72°C for 40 cycles; *Delta*/*Jagged* analysis, 30 s at 95°C, 30 s at 58°C, and 1 min at 72°C for 45 cycles. The PCR products were separated on a 1% gel, stained with ethidium bromide, purified, and sequenced. For primers, see (*7*).
19. T. L. Fletcher, P. De Camilli, G. Banker, *J. Neurosci.* **14**, 6695 (1994); A. N. van den Pol, K. Obrietan, A. B. Belousov, Y. Yang, H. C. Heller, *J. Comp. Neurol.* **399**, 541 (1998).
20. Randomly selected neurons ($n > 6000$) were imaged and coded to conceal their identity during the measuring (*24*). Neurites longer than 10 μm were traced and counted as branches. Statistical significance was determined by *t* test. Branching of neurites is presented as branching index (number of branches divided by mean neurite length per neuron) analyzed at 9 DIV, which elucidates the different incidence of branching between control lacZ-transfected neurons and other transfected neurons (lacZ = 100%). LD cultures: Notch1 ICD = 144.5 ± 9.3% ($P = 0.003$), Notch2 ICD = 157.8 ± 12.5% ($P = 0.003$). HD cultures: Nmb = 43.0 ± 1.3% ($P = 0.004$), Nbl = 31.3 ± 5.6% ($P < 0.0003$), Dx = 24.0 ± 5.1% ($P < 0.000006$).
21. S. Jarriault *et al*., *Mol. Cell. Biol.* **18**, 7423 (1998); L. Li *et al*., *Immunity* **8**, 43 (1998).
22. B. Varnum-Finney *et al*., *Blood* **91**, 4084 (1998).
23. S. Wang *et al*., *Neuron* **21**, 63 (1998).
24. H. Qi *et al*., *Science* **283**, 91 (1999).
25. To generate stably transfected cell lines, we transfected NIH 3T3 cells with 20 μg of plasmids [pDelta1, pJagged1 (*35*); phJ1^{EC}myc, amino acids 1 to 1046 (*22*)] and selected with G-418 (0.8 mg/ml) in 10-cm plates. At least two separate cell pools were generated for each plasmid and assayed for the expression of transfected genes. For coculture assays, 3T3 cells were grown in DMEM/F-12 with N2 (Gibco) and 5% FBS (*24*) until confluence. Neurons growing on the cover slips (5 and 12 mm) were placed on top of the monolayer, facing the 3T3 cells, and maintained for 20 to 24 hours.
26. J. M. Verdi *et al*., *Curr. Biol.* **6**, 1134 (1996).
27. W. Zhong, J. N. Feder, M.-M. Jiang, L.Y. Jan, Y. N. Jan, *Neuron* **17**, 43 (1996); W. Zhong, M.-M. Jiang, G. Weinmaster, L. Y. Jan, Y. N. Jan, *Development* **124**, 1887 (1997); Y. Wakamatsu, T. M. Maynard, S. U. Jones, J. A. Weston, *Neuron* **23**, 71 (1999).
28. K. Matsuno *et al*., *Nature Genet.* **19**, 74 (1998).
29. P. Ordentlich *et al*., *Mol. Cell. Biol.* **18**, 2230 (1998).
30. G. A. Dunn, *J. Comp. Neurol.* **143**, 491 (1971); P. Rakic, *ibid.* **146**, 335 (1972); V. H. Perry and R. Linden, *Nature* **297**, 683 (1982).
31. E. Giniger, *Neuron* **20**, 667 (1998); E. C. Olson *et al*., *Mol. Cell. Neurosci.* **12**, 281 (1998); R. Yavari, C. Adida, P. Bray-Ward, M. Brines, T. Xu, *Hum. Mol. Genet.* **7**, 1161 (1998); O. Berezovska *et al*., *Neuroscience* **93**, 433 (1999); P. Castella, J. A. Wagner, M. Caudy, *J. Neurosci. Res.* **56**, 229 (1999).
32. D. Price and S. S. Sisodia, *Annu. Rev. Neurosci.* **21**, 479 (1998).
33. O. Berezovska *et al*., *Mol. Brain Res.* **69**, 273 (1999); B. De Strooper *et al*., *Nature* **398**, 518 (1999); W. Song *et al*., *Proc. Natl. Acad. Sci. U.S.A.* **96**, 6959 (1999); G. Struhl and I. Greenwald, *Nature* **398**, 522 (1999); Y. Ye, N. Lukinova, M. Fortini, *ibid.*, p. 525.
34. P. Zagouras, S. Stifani, C. M. Blaumueller, M. L. Carcangiu, S. Artavanis-Tsakonas, *Proc. Natl. Acad. Sci. U.S.A.* **92**, 6414 (1995).
35. G. E. Gray *et al*., *Am. J. Pathol.* **154**, 785 (1999).
36. Bromodeoxyuridine (BrdU) was administered by intraperitoneal injections (50 mg/kg body weight). The morning of vaginal plug was designated E0.

37. We thank R. Mann for making human Delta and Jagged plasmids; G. Weinmaster and C. Hicks for 88C and J59 antibodies; A. Israel for IC antibodies; E. Mitsiadis for mouse Notch and Jagged plasmids; J. McGlade for Numb and Numb-like plasmids; T. Kadesch for CBF1-luc and Deltex plasmids; E. Nestler and J. Chen for use of the luminometer; and M. Ding, M. Donoghue, T. Haydar, and P. Mellman for technical assistance. Supported by NIH grants NS14841 (P.R.) and NS26084 (S.A.-T.).

23 June 1999; accepted 26 August 1999

All-Inorganic Field Effect Transistors Fabricated by Printing

Brent A. Ridley, Babak Nivi, Joseph M. Jacobson*

A solution of cadmium selenide nanocrystals was used to print inorganic thin-film transistors with field effect mobilities up to 1 square centimeter per volt second. This mobility is an order of magnitude larger than those reported for printed organic transistors. A field effect was achieved by developing a synthesis that yielded discretely sized nanocrystals less than 2 nanometers in size, which were free of intimately bound organic capping groups. The resulting nanocrystal solution exhibited low-temperature grain growth, which formed single crystal areas encompassing hundreds of nanocrystals. This process suggests a route to inexpensive, all-printed, high-quality inorganic logic on plastic substrates.

According to Moore's Law, the number of transistors per microelectronic chip has doubled every 18 months. However, the cost of a chip per unit of area has remained relatively static for more than two decades. Hence, there is interest in developing printing techniques for microelectronics fabrication that are inexpensive, allow fabrication on plastic substrates, and can cover large areas. The primary focus to date has been on organic materials for solution-based printing (*1–3*). Solution processable organic semiconductors such as poly(3-hexylthiophene) have demonstrated field effect mobilities of ~0.1 $cm^2\ V^{-1}\ s^{-1}$ (*3*). Theoretical considerations (*4*) and experiments with vacuum-deposited organic semiconductors such as pentacene (*5*) indicate that the mobilities in organic semiconductors may be fundamentally limited to values on par with that of amorphous silicon: ~1 to 2 $cm^2\ V^{-1}\ s^{-1}$. Although solution-processed organic thin-film transistors (TFTs) have been incorporated in

The Media Laboratory, Massachusetts Institute of Technology, 20 Ames Street, Cambridge, MA 02139, USA.

*To whom correspondence should be addressed. E-mail: jacobson@media.mit.edu

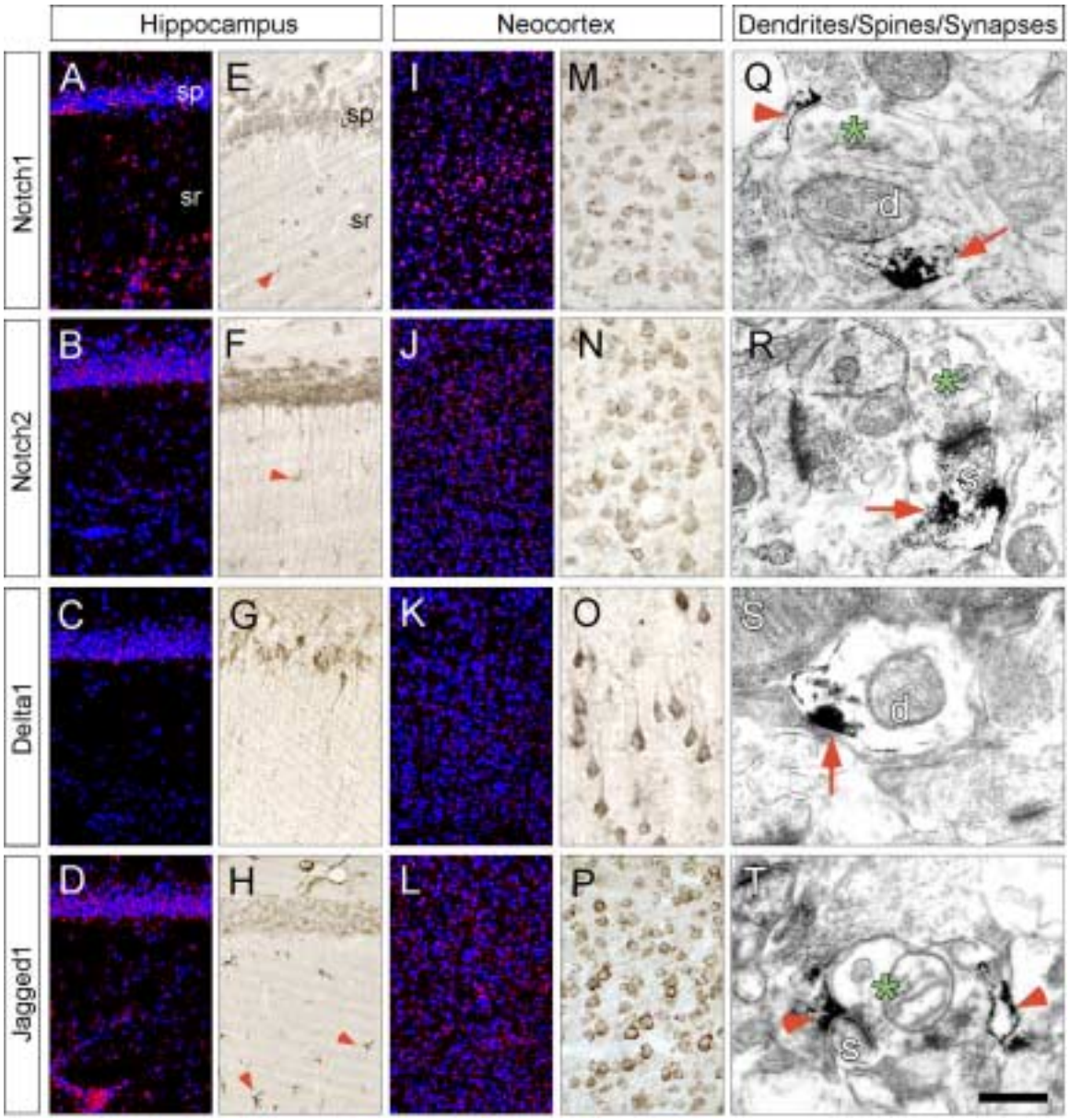

Figure 1: Notch, Delta, and Jagged are expressed in cortical neurons of the adult mouse brain. Representative regions, the CA1 region of the hippocampus and layers 3 to 5 of the somatosensory neocortex, are shown. (**A** to **D**, **I** to **L**) Dark-field autoradiographs of sections hybridized with Notch1, Notch2, Delta1, and Jagged1-specific ^{33}P-labeled antisense cRNAs (red) and counterstained with the DNA stain bisbenzimide (blue) (*n* = 5 brains). In situ hybridization was performed as described [M. J. Donoghue, R. M. Lewis, J. P. Merlie, J. R. Sanes, *Mol. Cell. Neurosci.* **8**, 185 (1996)]. In the hippocampus, the hybridization signals were associated with the cell bodies of pyramidal neurons in the stratum pyramidale (sp), and for Notch1, Notch2, and Jagged1 also with the cell bodies of astrocytes in the stratum radiatum (sr). (**E** to **H**, **M** to **P**) Representative micrographs showing the immunohistochemical localization of Notch1, Notch2, Delta1, and Jagged1 (*n* = 4 brains). Sections were processed in primary antibodies as described (*6*) and then incubated in biotinylated secondary antibodies (1:300; Jackson Immunoresearch) for 1.5 hours at room temperature, and developed using an ABC kit (Vector). Notch1 and Notch2 immunoreactivity are localized to the cell bodies and the proximal regions of apical and basal dendrites of pyramidal cells as well as interneurons and occasional axons. Delta1 and Jagged1 are also detected in neurons. The red arrowheads show immunolabeled glial cells. (**Q** to **T**) Micrographs show ultrastructural localization of Notch1, Notch2, Delta1, and Jagged1 immunoreactivity in proximal dendrites (d), dendritic spines (s), and synapses (asterisk, presynaptic terminal) of the somatosensory neocortex. The red arrowheads depict immunoelectron products in postsynaptic dendritic shafts and spines, whereas the red arrows depict immunolabeled glial processes ensheathing unlabeled presynaptic terminals and synapses. Note that the immunoelectron products are asymmetrically clustered; the opposing cellular elements contacting the immunoreactive cell parts are unlabeled. Scale bars, 70 µm (A to D, I to L), 50 µm (E to H, M to P), 220 nm (Q and S), 190 nm (R and T).

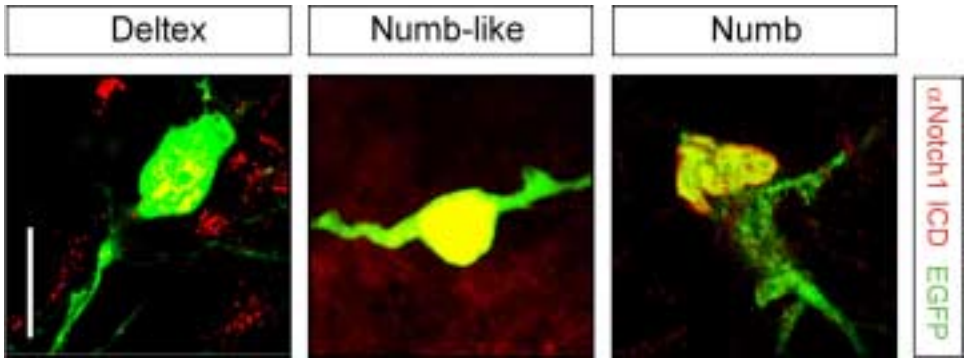

Figure 2: Numb, Numb-like, and Deltex do not prevent nuclear translocation of human Notch1 ICD. HD cultures were cotransfected with corresponding expression constructs (*12*) at 7 DIV and analyzed at 9 DIV. Representative confocal images illustrate the nuclear localization of Notch1 ICD epitopes (red/yellow) in $EGFP^+$ cells (green). Scale bar, 25 μm.

Supplemental Table 1. RT-PCR amplification sets. Primers were designed to span introns to test for genomic DNA amplification.

Gene	Primer	Sequence
hairy and Enhancer-of-split1	HES1A	5´-CAGCCAGTGTCAACACGACAC-3´
	HES1E	5´-TCGTTCATGCACTCGCTGAG-3´
hairy and Enhancer-of-split5	HES5C	5´-CGCATCAACAGCAGCATAGAG-3´
	HES5D	5´-TGGAAGTGGTAAAGCAGCTTC-3´
Glyceraldehyde 3-phosphate dehydrogenase	G3PDHA	5´-ACCACAGTCCATGCCATCAC-3´
	G3PDHB	5´-TCCACCACCCTGTTGCTGTA-3´
Delta-like1	D1A	5´-TACAGAAACACCAGCCTCCACCTGAAC-3´
	D1B	5´-TCTTGTATGTGGCTGACCATGAACCACAGG-3´
Jagged1	J1A	5´-TGCTTGGTGACAGCCTTCTACTGG-3´
	J1B	5´-GCC AAGTTCGAGACCCGTGAAAGG-3´
Jagged2	J2A	5´-GAAGCGCAGGAAAGAACGTGAGAG-3´
	J2B	5´-TGTAGGAACCACGAAGACTGCC-3´